Progress in Organic Coatings 93 (2016) 87–96

Contents lists available at ScienceDirect

Progress in Organic Coatings

journal homepage: www.elsevier.com/locate/porgcoat

UV-curable POSS-fluorinated methacrylate diblock copolymers for icephobic coatings

Kaiqiang Zhang [a], Xiaohui Li [a], Yunhui Zhao [a], Kongying Zhu [b], Yancai Li [a], Chao Tao [a], Xiaoyan Yuan [a,*]

[a] School of Materials Science and Engineering, and Tianjin Key Laboratory of Composite and Functional Materials, Tianjin University, Tianjin 300072, China
[b] Analysis and Measurement Center, Tianjin University, Tianjin 300072, China

ARTICLE INFO

Article history:
Received 23 October 2015
Received in revised form
11 December 2015
Accepted 8 January 2016

Keywords:
POSS
Fluorinated
Diblock copolymers
UV-cured coating
Icephobicity

ABSTRACT

Low surface energy materials have been extensively investigated for building icephobic surfaces in recent years. Polydimethylsiloxane (PDMS) and fluoropolymers have been introduced to this field, while control of their structures is of importance to produce deicing surfaces. In this work, fluorinated methacrylate block copolymers containing polyhedral oligomeric silsesquioxane (POSS) moieties were synthesized by reversible addition-fragmentation chain transfer polymerization and transformed into thiolated-copolymers by aminolysis to adjust the self-assembly and modify surface morphology. The icephobic coatings were developed *via* UV-curable thiol-ene reaction with tunable amounts of thiol-modified POSS-fluorinated methacrylate diblock copolymers with vinyl-functionalized PDMS and thiol-functionalized PDMS. Characterizations of atomic force microscopy, X-ray photoelectron spectroscopy, and contact angle showed the evidence of the POSS-fluorinated diblock copolymers on the outmost surface of the coatings. Owing to the crystallization of perfluoroalkyl side groups, the coatings containing thiol-modified poly(methacrylisobutyl POSS)-*b*-poly(2-perfluorooctylethyl methacrylate) (**S17F**) exhibited excellent icephobicity, and water droplets could rebound completely on all **S17F**-containing surfaces at both normal and tilt modes before freeze even at −15 °C. The ice shear strengths of the prepared UV-cured coatings were about one-eighth of that on bare aluminum surface, while the coating containing 5% **S17F** achieved the lowest ice shear strength of 105 ± 12 kPa. It was found that the icephobicity of these coatings were attributed primarily to the synergistic effect of the POSS-fluorinated methacrylate diblock copolymer and the PDMS component.

1. Introduction

Ice adhesion and accumulation on surfaces can bring about severe problems on telecommunication towers, wind turbines, aircraft wings, and ships [1–3]. To avoid the detrimental environmental consequences and substantial energy consumption caused by the active deicing methods, extensive investigations have been conducted to tailor inherent material properties for building icephobic surfaces via eliminating ice formation or reducing ice adhesion [3,4].

Most notably, fluoropolymers, ascribed to the low dielectric constant and low surface energy, have been widely utilized to prepare anti-icing and icephobic coatings [5–10], including fluoroalkylsilane [5], polytetrafluoroethylene (PTFE) [6,7] and poly(fluoroalkyl acrylate) [8–10]. Compared with PTFE, the flexible dangling fluoroalkyl groups of poly(fluoroalkyl acrylate)s can affect the molecular aggregation and the surface properties [8–14]. Particularly, with longer fluoroalkyl side groups, poly(fluoroalkyl acrylate)s exhibit crystallization properties, thus inhibit surface reorientation when contacting with water, which is important for hydrophobicity and icephobicity [8,11–14]. For example, poly(perfluorodecyl acrylate) can act as a steric barrier resisting local surface reorganization, forcing the reduction of undesirable contact angle hysteresis and low values of the ice adhesion strength [8]. Therefore, control of the molecular aggregation structure of fluoropolymers is an important issue for modifying the deicing surfaces.

Polyhedral oligonmeric silsesquioxanes (POSS) are molecules with special cage-like nano-scaled organic/inorganic hybrid structures [15–20]. Importantly, owing to suitable substituent groups, POSS and its derivatives are demonstrated to be easily incorporated into various hybrid polymers [16,17]. By

* Corresponding author at: School of Materials Science and Engineering, Tianjin University, Tianjin 300072, China. Tel.: +86 22 8740 1870 (O); fax: +86 22 8740 1870.
E-mail addresses: yuanxy@tju.edu.cn, xyuan28@yahoo.com (X. Yuan).

http://dx.doi.org/10.1016/j.porgcoat.2016.01.005
0300-9440/

copolymerization, methacrylisobutyl POSS (MAPOSS) has been used to modify the anti-wetting properties of coating materials, due to their low surface energy and hydrophobicity [18]. Expanding on utility, combining of fluorinated groups and POSS into synthetic materials, fluorodecyl POSS has been employed to tune surface energy and surface morphology for building icephobic films [19,20].

Owing to the incompatibility of block compositions, microphase separation could occur both in bulk and on surface of the block copolymers [9,10]. In a microphase-separated block copolymer, blocks with lower surface energy migrate to the surface preferentially [9,10,21]. With the developments of reversible addition-fragmentation chain transfer (RAFT) polymerization and atom transfer radical polymerization, well-architectured fluorinated block copolymers [9,13,21] and POSS-containing copolymers [17,18,22–26] have been obtained. Block copolymers containing POSS moieties are particularly attractive because they undergo self-assembly and microphase separation into block domains. Long-range structural ordering and hexagonally packed cylinders can be obtained by crosslinking of POSS-containing block copolymers [24]. On the other hand, anti-wetting coatings could be obtained by the self-assembly of fluorinated block copolymers due to their active self-orientation and self-migration to the surfaces [9,17,21]. Interestingly, in the previous work, we have found that nano-scaled morphologies obtained by the self-assembly and self-aggregation of block copolymers could be beneficial to icephobic coatings [9,10,26–28]. Fluorosilicone block copolymers polydimethylsiloxane-*b*-poly(fluorinated acrylate) [9], POSS-containing fluorosilicone block copolymers [10,18,26,27] and polymethyltrifluoropropylsiloxane-polyacrylate [28] have been synthesized in our lab, and the crosslinked coatings exhibited significant reduction in ice shear strength. Combining both POSS and fluoropolymer by RAFT polymerization, the advanced POSS-fluorinated diblock copolymers with extraordinary surface properties are expected.

UV-curing is an efficient method to produce crosslinked materials, due to the rapid curing rate at ambient temperature, as well as low energy consumption [29–32]. It has been reported that the fluoride-containing POSS [29] and fluorinated copolymers [30] can migrate onto the surface and decrease the interface energy between UV-curable liquid acrylate resin and air. Attributed to the insensitivity to oxygen inhibition, thiol-ene reaction has also been explored in the development of crosslinked surface [31,32].

Inspired by the above successful strategies against ice adhesion and the effective UV-curing method, in this research, POSS-fluorinated diblock copolymers were initially synthesized by RAFT polymerization involving methacrylisobutyl POSS (MAPOSS) and perfluorooctyl methacrylate (13FMA) or 2-perfluorooctylethyl methacrylate (17FMA). The dithioester ends of the prepared copolymers were transformed into thiol groups and then blended with vinyl-functionalized PDMS (PDMS-V) and thiol-functionalized PDMS (PDMS-SH) for preparation of UV-cured coatings. PMAPOSS was introduced for improving hydrophobicity and the miscibility with PDMS component. The fluorinated methacrylate, 13FMA or 17FMA, was architected as the second block for facilitating block copolymers to migrate onto the surface. The morphologies and surface chemical compositions of the copolymer coatings as well as the effect of the POSS and fluorinated block on icephobic properties were investigated.

2. Experimental methods

2.1. Materials

Methacrylisobutyl POSS (MAPOSS) was purchased from Hybrid Plastics, USA, and used as received. Perfluorooctyl methacrylate

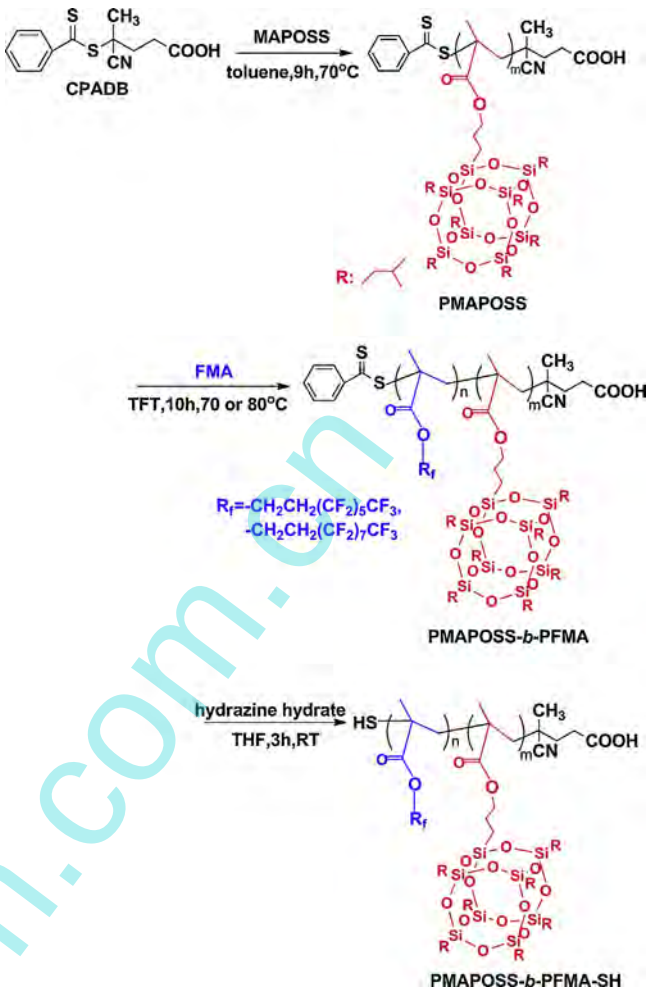

Scheme 1. Synthesis of thiol-terminated PMAPOSS-*b*-PFMA-SH *via* RAFT polymerization.

(13FMA) and 2-perfluorooctylethyl methacrylate (17FMA) were supplied by Xeogia Fluorin-Silicon Chemical Co., Ltd., China, and purified by passing over a column of alumina to remove inhibitor. Vinyl-functionalized PDMS (PDMS-V) (1.7 wt% of vinyl content M_n = 24,000) was obtained from Shandong Dayi Chemical Co., Ltd., China, and thiol-functionalized PDMS (PDMS-SH) (2.7 wt% of thiol content, M_n = 6000) was purchased from Shanghai Winner Silcone Materials Co., Ltd., China. 4-Cyanopentanoic acid dithiobenzoate (CPADB) was synthesized according to the reference [33]. 2,2′-Azobisisobutyrobutyl acrylate (AIBN) was obtained from Tianjin Kemiou Chemical Reagent Co., Ltd., China, and used after recrystallization by ethanol. Dimethylphenylphosphine (Me_2PPh) was obtained from Aladdin industrial Inc., China. Photoinitiator of 2,2-dimethoxy-2-phenylacetophenone (DMPA) was obtained from J&K Chemical Ltd., China. Tetrahydrofuran (THF), α,α,α-trifluorotoluene (TFT) and hydrazine hydrate (N_2H_4) were purchased from Tianjin Heowns Biochem Technologies LLC, Tianjin, China, and used without further purification.

2.2. Synthesis of POSS-fluorinated methacrylate block copolymer

POSS-fluorinated methacrylate block copolymers were synthesized by RAFT polymerization (Scheme 1). Briefly, MAPOSS (2.12 g, 1 mmol), CPADB (0.0417 g, 0.07 mmol) and AIBN (8.19 mg, 0.02 mmol) were dissolved into 4 mL of anhydrous toluene and placed in a 25-mL Schlenk tube which was thoroughly deoxygenated by five consecutive freeze-pump-thaw cycles. The tube

was immersed in an oil bath at 70 °C and the polymerization was carried out for 9 h under argon atmosphere. The obtained poly(methacrylisobutyl POSS) (PMAPOSS) was purified by precipitation in methanol and dried in a vacuum oven overnight for uses as macro chain transfer agent for further RAFT polymerization.

The POSS-fluorinated diblock copolymers, i.e., poly-(methacrylisobutyl POSS)-*b*-poly(perfluorooctyl methacrylate) (PMAPOSS-*b*-P13FMA) or poly(methacrylisobutyl POSS)-*b*-poly(2-perfluorooctylethyl methacrylate) (PMAPOSS-*b*-P17FMA) were prepared from PMAPOSS and 13FMA or 17FMA. Typically, PMAPOSS (0.30 g, 1 mmol), 13FMA (0.40 g, 25 mmol) or 17FMA (0.40 g, 15 mmol) and AIBN (2.04 mg, 0.33 mmol) were dissolved in 1.8 mL of TFT and placed in Schlenk tube which was thoroughly deoxygenated by five consecutive freeze-pump-thaw cycles. The tube was subsequently placed in an oil bath, (70 °C for the polymerization of 13FMA, and 80 °C for the polymerization of 17FMA) for 10 h and stirred under argon atmosphere. After polymerization, the block copolymer was precipitated into methanol and dried under vacuum.

The thiol-modification of **S**, **S13F**, **S17F** (**S**, **S13F** and **S17F** are designated as sample PMAPOSS-SH, PMAPOSS-*b*-P13FMA-SH and PMAPOSS-*b*-P17FMA-SH, respectively) were prepared according to the references [34,35]. Typically, PMAPOSS (0.30 g, 0.053 mmol), [PMAPOSS-*b*-P13FMA (0.53 g, 0.053 mmol) or PMAPOSS-*b*-P17FMA (0.54 g, 0.053 mmol)] was dispersed in 20 mL THF with hydrazine (10.0 μL 0.53 mmol) and Me_2PPh (8.0 μL, 0.11 mmol). The solution was stirred for 3 h at room temperature under N_2 protection. Then, the solution was precipitated into methanol (900 mL) and dried in vacuum overnight.

2.3. Preparation of UV-cured coatings

Thiol-ene UV-cured coatings were prepared by weighing the desired ratio of PDMS-SH, PDMS-V, DMPA and the thiol-terminated polymers (**S**, **S13F**, or **S17F**) into a glass jar (detailed in Table S1). Then, the blend ingredients were dispersed in TFT/THF mixed solution (4:1 w/w solvent/blends) by ultrasonication for 30 min. The coatings were prepared by spin-coating at 600 rpm (5 s) and 3000 rpm (10 s) for the first and second steps, respectively, on polished aluminum plates (20 mm × 20 mm) and cured under a UV flood lamp (2.5 mW/cm^2 spectronics US) for 15 min. Incorporated with three series copolymer, the coatings were denoted as **S-*y***, **S13F-*y*** and **S17F-*y*** (***y*** = 1, 3, 5, 10, 20, 30, and 40 wt% copolymer with respect to PDMS-V). Without the addition of any copolymers, the UV-cured coating (**SF-0**) was prepared as a control.

2.4. Characterization

The relative molar mass and polydispersity index (PDI) of the prepared POSS-fluorinated methacrylate block copolymers which determined in a Waters 1515-2414 gel permeation chromatography (GPC) are summarized in Table 1. The flow rate was 1 mL of THF/min at 40 °C. UV–vis spectra were recorded on an ultraviolet-visible spectroscopy (UV-2450, Shimadzu, Japan).

Table 1
Compositions of PMAPOSS, PMAPOSS-*b*-P13FMA and PMAPOSS-*b*-P17FMA, and their molecular weights.

Sample	$\overline{M}_{n\mathrm{NMR}}$	$\overline{M}_{n,\mathrm{GPC}}$	$\mathrm{DP}_{\mathrm{MAPOSS}}$[a]	$\mathrm{DP}_{\mathrm{FMA}}$[a]	W_F[b] (wt%)	PDI
PMAPOSS	9200	5160	10	–	–	1.08
PMAPOSS-*b*-P13FMA	16,500	5797	10	17	0.25	1.11
PMAPOSS-*b*-P17FMA	16,600	6592	10	14	0.26	1.14

[a] Measured by ^{1}H NMR after purified.

[b] $W_F = \left(M_{\mathrm{FMA}} \times \mathrm{DP}_n / M_{n,\mathrm{NMR}}\right) \times F$, where, F (wt%) represents the fluorine element content in FMA.

Fourier transform infrared spectra (FT-IR) were recorded in a Perkin-Elmer Spectrum 100. Polymer coatings were cast on KBr pellets for the measurement. Proton-nuclear magnetic resonance (^{1}H NMR) analysis was carried out in Varian machines (INOVA 500 MHz and Infinity plus 300WB, USA) by dissolving the samples in deuteriochloroform. Differential scanning calorimetric analysis (DSC) was performed with a Perkin-Elmer Diamond differential scanning calorimeter under a dry nitrogen atmosphere with a heating rate of 10 K/min and heated from 0 °C to 180 °C. Transmission electron microscope (TEM) images were recorded in a JEOL JEM100CXII machine operated at 100 kV. A droplet of each copolymer solutions (1 wt% in TFT/THF, TFT:THF = 50:50) was deposited on a carbon-coated copper grid and allowed to evaporate at room temperature for 24 h.

The aggregation states of coating surfaces were determined by X-ray diffraction (XRD) (D/max 2500 machine, λ = 0.154 nm, scattering angle 2θ = 3–50°). Surface composition by X-ray photoelectron spectroscopy (XPS) was estimated using a Perkin-Elmer PHI 5000C ECSAX-ray photoelectron spectroscope in ultra-high vacuum with Al K radiation (1486.6 eV) operating at 24.2 W under a vacuum less than 5×10^{-8} Torr at 45°. Atomic force microscope (AFM) images were obtained using tapping mode on a CSPM5500A machine (Being Nano-Instruments Ltd., Guangzhou, China) equipped with E-type vertical engage piezoelectric scanner. The AFM samples were prepared onto freshly cleaved silicon wafer surfaces by spin-coated, in accordance with earlier method. An average thickness of 100 nm was observed for the spin-coated coatings.

Static contact angle, advancing angle and receding angle were measured using a JC2000D contact angle meter (Shanghai Zhongchen Equipment Ltd., China). All the presented contact angle values are averages of five or six measurements. The surface energies of polymers and coatings were evaluated by measuring static water and hexadecane contact angles on the surface and were calculated according to the equation by Owens–Wendt–Kaelble method [36].

Dynamic flow of water onto the test coatings was detected by high-speed video camera (Olympus *i*-speed LT 4GB color Japan). The coated Al plate kept at controlled temperatures (20 °C or −15 °C), and positioned at fixed angles of 0° or 30° to the horizontal. Water droplets (7 μL) at room temperature or 0 °C, were dropped onto sample surfaces from 5 cm or 10 cm height [37]. N_2 was used to keep the environment in the desiccator chamber dry and reduce condensation on the substrates.

Ice shear strength was measured within a custom-made humidity-controlled chamber in a low-humidity nitrogen atmosphere equipped with a force transducer (Model ZP-500, Imada, Japan) in a push mode. The push velocity was controlled at a constant rate of 0.5 mm/s by using a motion stage (Liansheng, Jiangxi, China). The glass columns were put on the Al plate sample and filled in 450 μL of fresh deionized water. Each column had a contact area with the sample of approximately 78.5 mm^2. The cooling stage was covered by an organic glass box which was purged with nitrogen gas to decrease the humidity. The temperature of the cooling plate was cooled at a rate of 2 °C/min and frozen at −15 °C for 3 h for complete ice formation before tests [18,28].

3. Results and discussion

A lot of works have been done in developing icephobic coatings, and silicone as well as fluoropolymers has been used in this field. In order to explore a facile way to produce feasible coatings with icephobic property, we adopt the UV-cured technique. Without expensive platinum catalyst and thermal-initiated free radical reaction, the UV-cured coatings

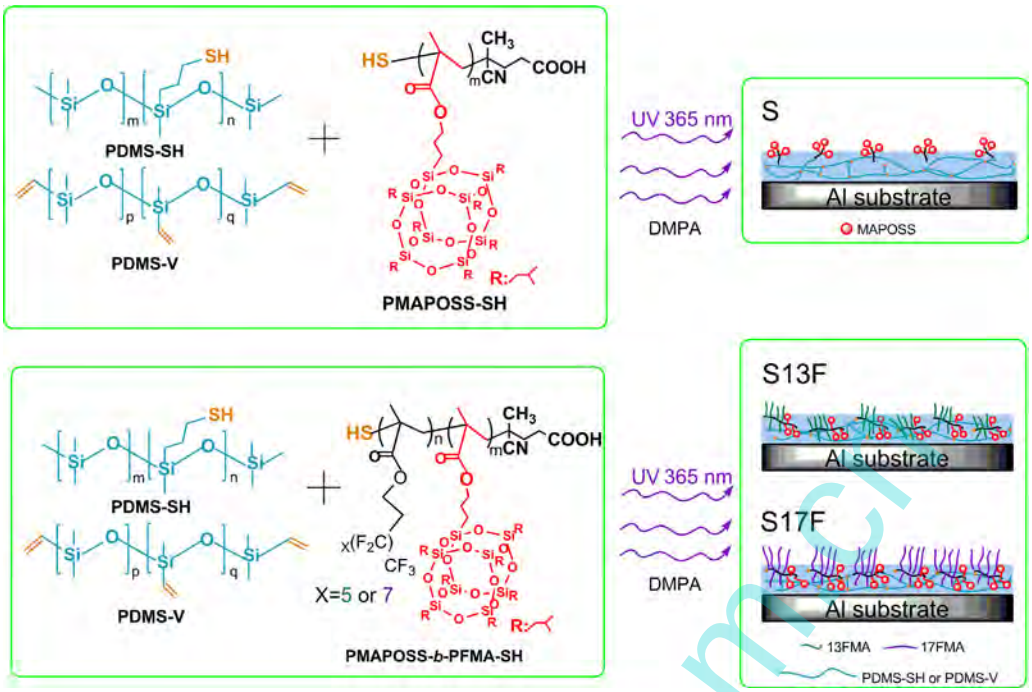

Fig. 1. Schematic illustration of formation of the icephobic coatings from UV-curable POSS-fluorinated methacrylate diblock copolymers. PMAPOSS aggregates have bloomed to the surface during spin-coating and UV-curing in PMAPOSS-SH (**S**) containing surface. Attributed to more excellent surface migration of fluorine segments, the agglomeration of PMAPOSS was suppressed and fluorinated polyacrylate blocks were observed in PMAPOSS-*b*-P13FMA-SH (**S13F**) and PMAPOSS-*b*-P17FMA-SH (**S17F**) containing surface.

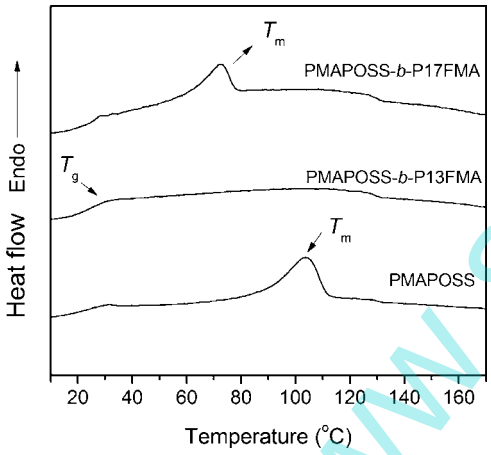

Fig. 2. DSC curves of PMAPOSS, PMAPOSS-*b*-P13FMA and PMAPOSS-*b*-P17FMA.

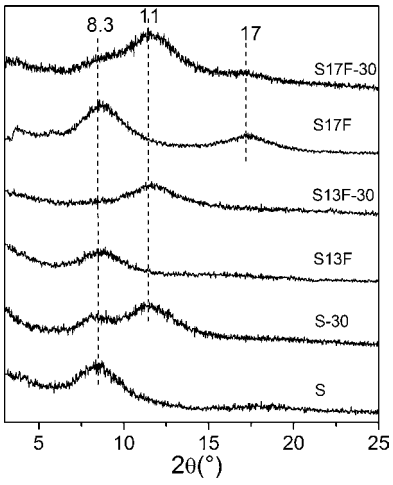

Fig. 3. XRD curves of block copolymers (**S**, **S13F** and **S17F**) and UV-cured coatings (**S-30**, **S13F-30** and **S17F-30**).

were prepared via thiol-ene reaction using POSS-fluorinated methacrylate diblock copolymers, PDMS-V and PDMS-SH. PDMS was chosen as the main component for the icephobic coatings due to the extremely low-glass transition temperature (−123 °C), low surface tension and surface energy [4,38]. By varying the additives and incorporation amount of POSS-fluorinated diblock copolymers, coatings with different performance could be acquired. The whole strategy to fabricate the UV-cured surfaces (**S-*y***, **S13F-*y*** and **S17F-*y***) is illustrated in Fig. 1.

3.1. Thermal and crystallization behaviors of the prepared copolymers and UV-cured coatings

Indicative ^{1}H NMR and FT-IR spectra of the POSS-fluorinated methacrylate diblock copolymers are given in the supplementary data Figs. S1 and S2, respectively, to validate the polymer synthesis successfully. And the isolation of thiol-terminated copolymer was conveniently confirmed using a combination of UV–vis spectrophotometry and GPC curves as shown in the supplementary data Fig. S3. The thiol-ene reaction confirmed by FT-IR spectra is given in the supplementary data Fig. S4. Disappearance of the peak at 2580 cm^{-1} indicates that the thiol groups have reacted with enes to generate the crosslinked structure.

In representative DSC curves (Fig. 2), the melting temperature (T_m) at 105 °C was measured, proves to be slight crystallization of PMAPOSS copolymer. For PMAPOSS-*b*-P13FMA block copolymers, the presence of P13FMA blocks hindered the aggregation of PMAPOSS, thus, inhibits the crystallinity of the PMAPOSS component, and no T_m was detected. The DSC curves revealed melting peak at 75 °C for the copolymer PMAPOSS-*b*-P17FMA, in accordance with that of a crystalline structure formed by the 17FMA perfluoroalkyl side groups [14].

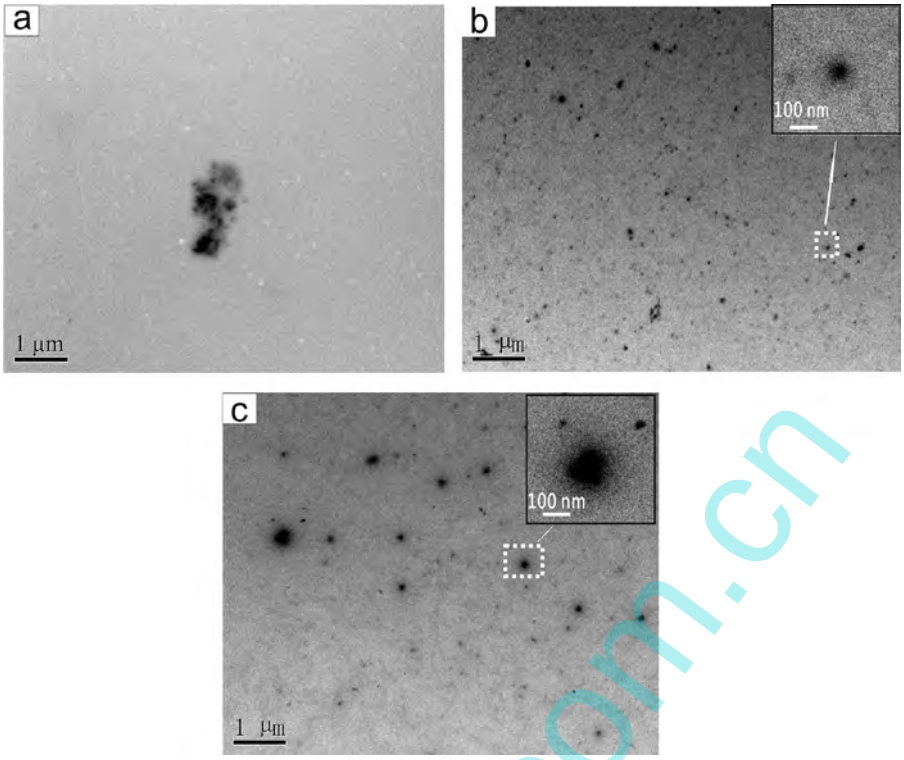

Fig. 4. TEM images of PMAPOSS (a), PMAPOSS-*b*-P13FMA (b), and PMAPOSS-*b*-P17FMA (c).

Table 2
Element compositions of the UV-cured coatings obtained by XPS analysis.

Sample	Element compositions (atomic%)				Bulk F/Si atomic ratio	Surface F/Si atomic ratio
	C	O	F	Si		
SF-0	53.6	24.4	–	21.9	–	–
S-5	52.8	26.6	–	20.7	–	–
S-30	50.9	25.9	–	23.3	–	–
S13F-1	52.9	23.9	1.5	21.8	0.003	0.06
S13F-3	52.4	23.9	2.3	21.5	0.008	0.11
S13F-5	52.1	24.1	3.3	20.6	0.01	0.16
S13F-10	51.5	25.5	3.0	20.0	0.03	0.15
S13F-20	51.3	24.9	3.6	20.3	0.07	0.17
S13F-30	52.1	23.8	6.1	18.0	0.09	0.33
S13F-40	55.3	22.3	6.2	16.2	0.14	0.38
S13F	51.5	15.9	25.3	7.3	1.87	3.46
S17F-1	48.4	22.1	12.9	16.7	0.003	0.77
S17F-3	48.7	22.4	13.2	15.8	0.008	0.83
S17F-5	47.1	21.8	15.9	15.3	0.01	1.03
S17F-10	48.7	22.4	13.0	15.9	0.03	0.81
S17F-20	45.8	19.2	20.7	14.3	0.07	1.44
S17F-30	46.9	16.4	26.6	10.1	0.10	2.63
S17F-40	45.4	14.0	32.4	8.3	0.14	3.90
S17F	44.6	10.1	40.7	4.6	1.90	8.84

To evaluate the molecular aggregation states of the copolymers and UV-cured coatings, the XRD measurement was performed and the resulting diffraction profiles are shown in Fig. 3. Peaks were observed at 8.3° which were assignable to the packing of POSS structures in **S**, **S13F** and **S17F** copolymers. Compared with **S13F**, peaks at 17° were found owing to the crystallinity of longer perfluoroalkyl side groups in **S17F** block copolymer [14]. For UV-cured coatings, attributed to an amorphous halo of PDMS, the diffractions at around $2\theta = 11°$ became obvious. Although only a little mass proportion added relative to the PDMS component, peaks at 8.3° assignable to the packing of POSS structures can be found in **S-30** coating. Although not obvious, peaks at 17° assignable to the packing of P17FMA also can be found in **S17F-30** coating, which indicate the molecular aggregation of P17FMA block copolymers to coating surface. From DSC and XRD measurements, we could find that PMAPOSS tended to form agglomeration structure. With the addition of fluorinated block, the agglomeration structure of PMAPOSS was significantly weakened. It has been revealed that compared to **S13F** block copolymers, perfluoroalkyl side groups in P17FMA block was in the crystalline state and formed ordered structures at the surface [11,12], which could enhance the surface aggregation of **S17F** block copolymers.

3.2. Surface composition and morphology

The bulk morphologies of the copolymers were verified by TEM study (Fig. 4). Aggregates of PMAPOSS with diameter approximate 500 nm are clearly seen in Fig. 4(a). By the introduction

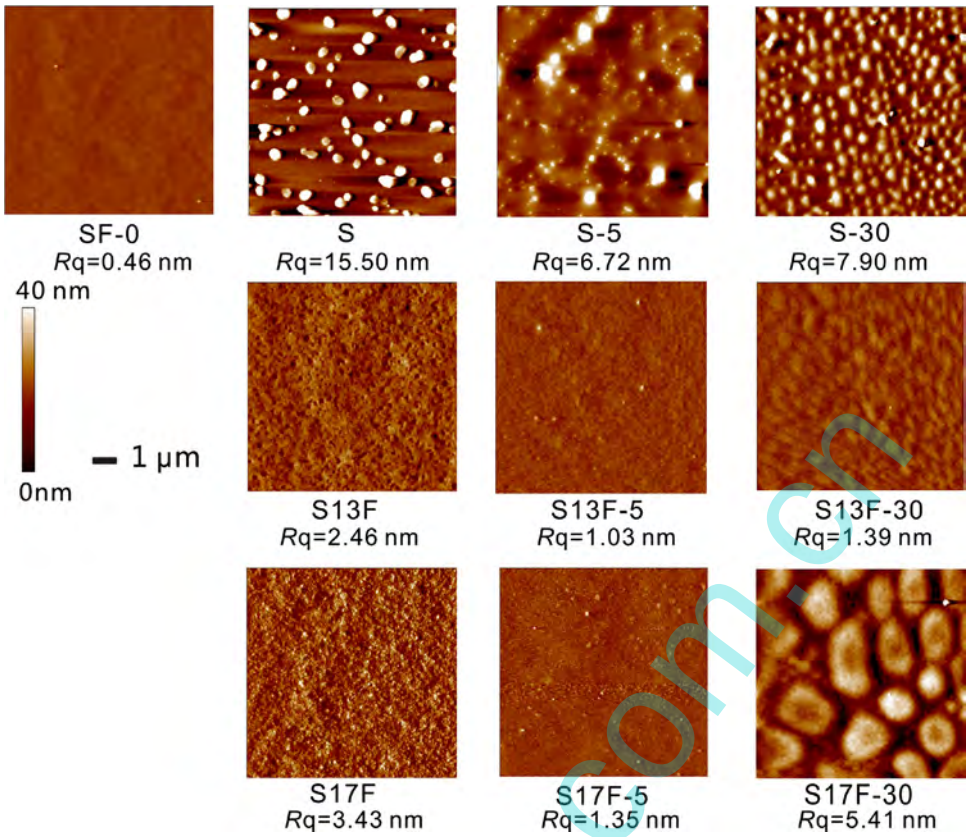

Fig. 5. AFM images of block copolymers (**S**, **S13F** and **S17F**) and UV-cured coatings over a scope of 10 μm × 10 μm.

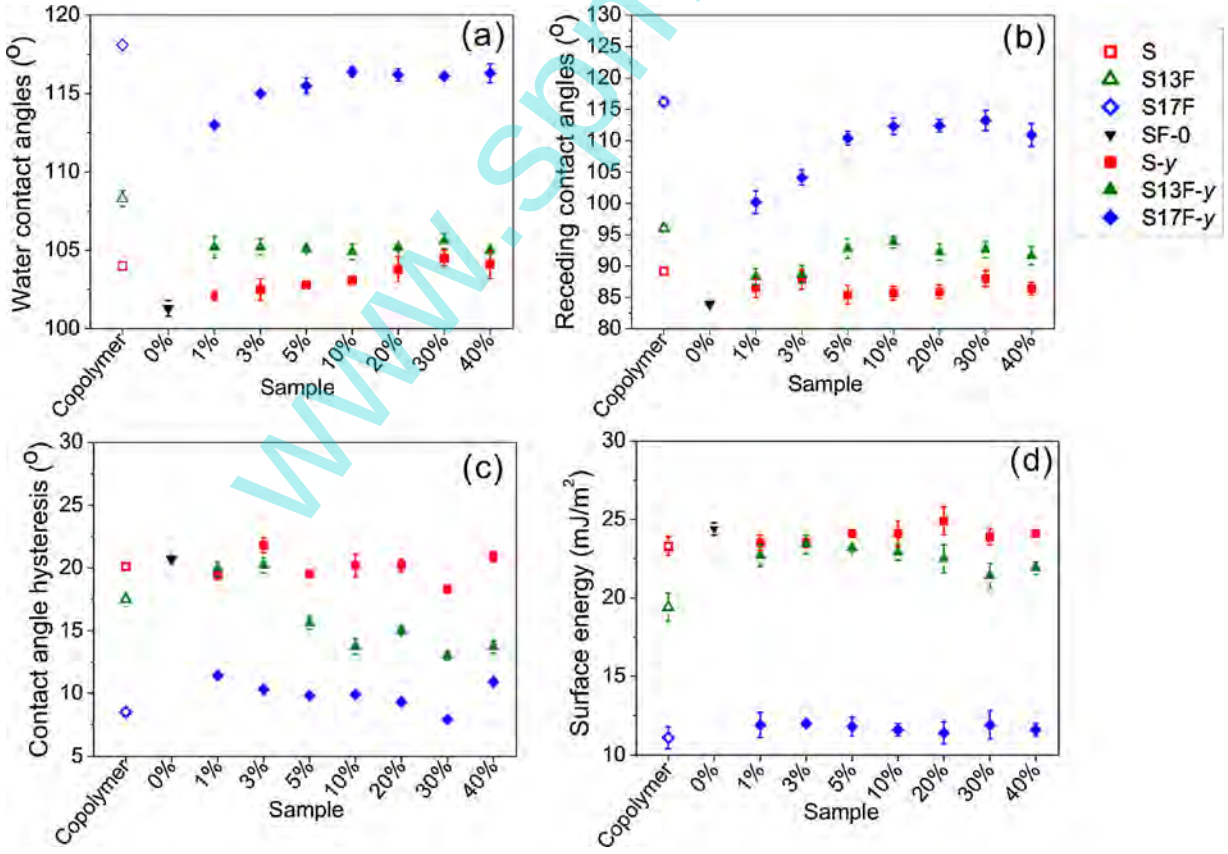

Fig. 6. Water contact angles (a), receding contact angles (b), contact angle hysteresis (c), and surface energies (d) of the diblock copolymers and their UV-cured coatings (***y*** = 1, 3, 5, 10, 20, 30 and 40).

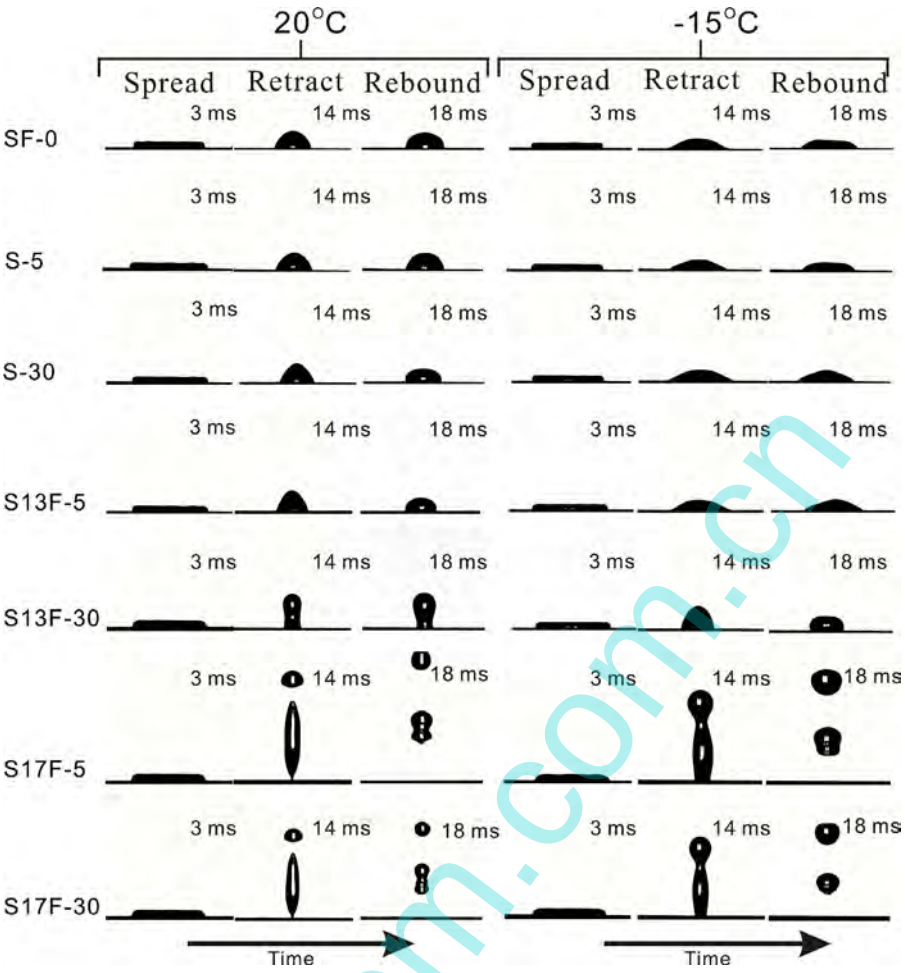

Fig. 7. Images of the dynamic behavior of 7 μL, room temperature or 0 °C water droplet impacting on the horizontal surface of UV-cured coatings from a 10 cm height at 20 °C or −15 °C.

of the P13FMA or P17FMA block, self-assembled micelles of PMAPOSS-*b*-P13FMA (diameter about 30–100 nm) and PMAPOSS-*b*-17FMA (diameter about 100–300 nm) are observed.

Characteristic signals of carbon, oxygen, fluorine and silicon are found in the XPS spectra for the UV-cured surfaces, and the full elemental analyses were shown in Table 2. With the addition of PMAPOSS-SH (**S**) into curing process, no significant variation in surface chemical composition was detected, due to the similar Si–O structures between PDMS and MAPOSS. The self-segregation of fluorine-containing groups at the surface is more pronounced than that of silicon-containing groups, resulting in a higher density of fluorine at the surface than in the bulk. Therefore, with the addition of copolymer **S13F** or **S17F**, the F/Si ratios on the coating surfaces by XPS analyses in Table 2 are obviously higher than the theoretical values calculated from the chemical formula of monomers for the bulk. With the almost same content of block copolymer, the enrichment of fluorine was more significant on the **S17F**-containing coatings than that of **S13F**-containing ones. Compared with **S13F-30** surface (6.1 wt%), the fluorine content of **S17F-30** surface (26.6 wt%) is higher. This result is also in line with the XRD and DSC results, which suggests the migration and crystallization of P17FMA onto the surface.

The surface morphologies of the block copolymers and the UV-cured coatings were investigated by AFM in Fig. 5. In **S** sample, PMAPOSS aggregates (bright regions) have bloomed to the surface during the spin coating and solvent evaporation, and the root-mean-square roughness (R_q) of 15.5 nm was observed. Due to the self-assembly of POSS-fluorinated methacrylate blocks and the more excellent surface migration of fluorine segments, the agglomeration of PMAPOSS was suppressed in **S13F** and **S17F** samples, and R_q were reduced to 2.46 nm and 3.43 nm, respectively. These results of AFM could be favorably compared with TEM and the XPS analysis, in which the smaller micelles formed and the fluorine content on surfaces of **S13F** (25.3%) and **S17F** (40.7%) are obviously higher. It is believed that the microphase separation topologies of block copolymers are related closely to their self-assembled properties by migrating different segments onto the coating surface.

For the UV-cured coatings (Fig. 5), these morphological features were reorganized during the UV-cured crosslinking process. The **SF-0** surface is relatively smooth, with the roughness R_q less than 0.5 nm. On the contrary, attributed to the presence of PMAPOSS aggregates, which are more likely to cluster and migrate onto the topmost surface, raised spherical structures can be still found in **S-5** and **S-30** samples. By taking advantages of the migration of POSS-fluorinated blocks (**S13F** and **S17F**) and conquering the barrier of PDMS, microphase-separated surface structures were brought about in **S13F-*y*** and **S17F-*y*** samples, especially for **S13F-30** and **S17F-30**. Compared with **S13F-30**, in **S17F-30** sample, brighter island areas assigned to **S17F** phase appeared. The evolution of the surface morphology with the increased amount of **S17F**

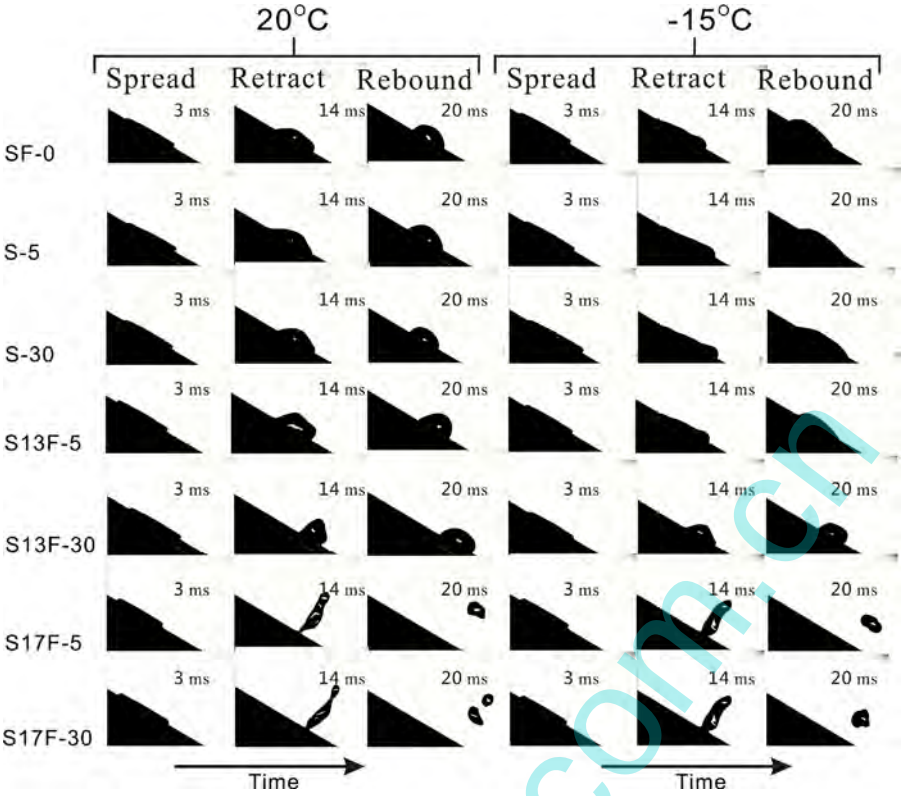

Fig. 8. Images of the dynamic behavior of 7 μL, room temperature or 0 °C water droplet impacting on a 30° inclined surface of UV-cured coatings from a 10 cm height at 20 °C or −15 ° C.

can be attributed to the enrichment of P17FMA segments at the surface–air interface and the reorganization of PDMS phase, which was also confirmed by XRD and XPS.

3.3. Wettability

To assess the hydrophobicity of the UV-cured coating, dynamic water contact angles measurements were conducted, including static water contact angle (WCA), advancing contact angles (θ_a), and receding contact angles (θ_r), contact angle hysteresis (CAH) and surface free energy. As we know, both surface morphology and composition have influences on WCA, θ_a, and θ_r. However, the AFM observation of the surface revealed the roughness is small, indicating that the effect of physical roughness on the contact angle can be negligible [11,12]. Therefore, the difference in surface wetting behavior should be mainly attributed to the surface chemical composition. Obviously, as shown in Fig. 6, all the UV-cured coatings exhibited WCA above 102°. With the incorporation of P13FMA, samples **S13F-*y*** showed higher values of WCA and θ_r than **S-*y***, because more hydrophobic P13FMA blocks could migrate to the surface of the coatings, as confirmed by XPS detection and AFM observation. Among **S13F-*y*** coatings, **S13F-30** presented higher WCA 105 ± 0.7°, less CAH 13 ± 0.9° and lower surface energy 21.4 mJ/m^2.

For the samples with the addition of P17FMA blocks into copolymer, the surface energy of **S17F-*y*** coatings decreases drastically, which was in accordance with the increasing of the fluorine content in XPS results. As shown in Fig. 6, the WCA above 113 ± 0.5°, the CAH below 11.0 ± 0.9° and the surface energy about 11.2 mJ/m^2 were detected for all **S17F-*y*** samples, even with 1 wt% weight **S17F** loading (**S17F-1**). Apart from the lower surface energy of **S17F-*y*** coatings, the mobility of molecular chains is an important factor in determining wetting behavior [11,12]. In the case of **S17F**, because of the stability and the crystallization of perfluoroalkyl side groups, which confirmed by XRD and DSC, the mobility of the molecular chains is restricted, lowing the reorientation of the perfluoroalkyl chains and the exposure of the polar groups (carbonyl groups) in contact with water. This can explain the receding contact angles of **S17F-*y*** coatings increased above 100° significantly.

3.4. Water impact and icephobic performance on the surfaces

In the present work, the water droplets impacting behaviors involving spreading, retracting, and rebounding on the UV-cured coating surfaces were investigated (Figs. 7 and 8). For **SF-0**, **S-5**, and **S-30** samples, retraction was limited and rebounding behavior was negligible, regardless of surface at horizontal surface or inclined at 30°. With the addition of fluorine-containing contents, more obvious droplets retraction can be found in **S13F-5** and **S13F-30** samples. But the retracted droplets remained pinned and did not fully withdraw from the surface, followed by several slight horizontal vibrations until the energy depleted. However, for **S17F-5** and **S17F-30**, the droplets can absolutely rebound at room temperature. The higher receding contact angle above 110° is the key wetting parameter that influences drop rebound, along with surface hydrophobicity. According to Antonini's study [39], rebound was observed only on surfaces with receding contact angles higher than 100°, that consistent with our results. It should be noticed that, at low temperatures, the retraction behavior of droplet can be affected by an increasing liquid viscosity [37,40]. It is seen that compared to the situation at ambient temperatures, lower substrate temperatures (−15 °C) lead to lesser droplets retraction for **SF-0**, **S-5**, **S-30**, **S13F-5**, and **S13F-30** samples. However, the effect of temperature is completely negligible for the **S17F-*y*** hydrophobic samples. The droplets impacting on **S17F**-containing coatings can fully retract and leave the surface within 20 ms. In addition, the

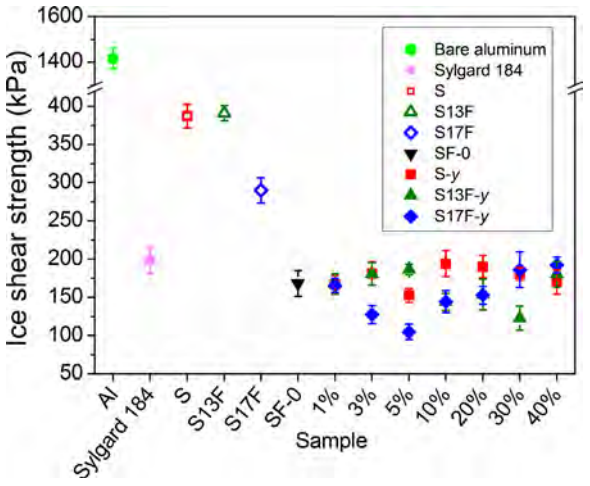

Fig. 9. Ice shear strength of block copolymers and UV-cured coatings (***y*** = 1, 3, 5, 10, 20, 30 and 40).

dynamic behaviors of water droplets impacting on the horizontal or 30° inclined **S17F-5** surface from 5 cm height were also conducted (Fig. S5). It can be seen that the time of retraction process increased from 14 ms at 10 cm to 20 ms at 5 cm due to the decreased kinetic energy of water droplet [41,42]. However, the energy dissipation of the water droplet is still small and the complete retraction of water can also be observed. Therefore, large receding contact angle above 100° in the retraction phase means high droplet mobility which ensures that the droplets can rebound from the UV-cured coating and impacting supercooled droplets did not nucleate. Hence, the surface can be considered as icephobic under these test conditions.

The ice shear strength was also measured to explore the icephobic property of the UV-cured coating. As shown in Fig. 9, without the main ingredients PDMS, the higher ice shear strength above 290 kPa could be found in **S**, **S13F** and **S17F** copolymer coatings. Meanwhile, lack of the addition of POSS-fluorinated copolymer, the **SF-0** sample could only present the ice shear strength slightly lower than commercial Sylgard 184. However, coated with POSS-fluorinated copolymer and functional PDMS, the ice shear strength was almost below 200 kPa, significantly reduced by more than eight-fold compared to the aluminum plates (1417 ± 25 kPa). It should be noted that the synergetic effects between POSS-fluorinated diblock copolymers and PDMS component resulted in preventing ice adhesion. The low T_g of PDMS infers the flexibility at low temperature and makes UV-cured coating "softer". The stiffness difference between ice and the sample surface can result in the concentrated stress building at the ice/coating interface to provide a path for easy ice release [4,43]. On the other hand, the low surface energy of POSS-fluorinated diblock copolymers is beneficial to reduce the strength of ice adhesion [4,5]. Therefore, compared with **S-*y*** coatings, the lower ice shear strength 123 ± 16 kPa was achieved in **S13F-30** coating. Attributed to the drastically decreased surface energy (11.2 mJ/m^2), the ice shear strength continue dropping to 105 ± 12 kPa on the **S17F-5** coating. But, with the increased adding amount of **S17F** block copolymers from 10 to 40 wt%, the ice shear strength slightly increased. This is because the migration of **S17F** suppressed the effect of PDMS, which can be confirmed by XPS. Different from superhydrophobic surfaces [4,5], the icephobicity of UV-curable coatings strongly depend on the synergism between the low surface energy of POSS-fluorinated diblock copolymers and PDMS component, rather than the surface roughness and the resulting trapped air between ice and textured surfaces. These findings are of great importance in the design of new types of icephobic coating.

4. Conclusions

Thiol-modified POSS-fluorinated diblock copolymers **S13F** and **S17F** were synthesized by RAFT polymerization, and then blend with PDMS-V and PDMS-SH for preparation of coatings by UV-curable technique based on thiol-ene functionality. Characterizations of morphology, surface chemical composition and water contact angles suggested that the block copolymers tended to migrate to the outmost surfaces as microphase separation happened in crosslinking process. As expected, the longer fluorinated side chains in **S17F** provided better hydrophobic performance than the shorter one in **S13F** due to the lower surface energy and the limited surface mobility, which prevents local remodeling of the surface. As compared with **S13F**-containing coatings, **S17F**-containing coatings presented higher WCA (113–116.5°), higher receding contact angles (100–113°), lower hysteresis of contact angle (8–11°) as well as lower surface energies (11.1–11.6 mJ/m^2).

It was found that water droplets could rebound completed on the **S17F**-containing surfaces even at −15 °C, indicating an active ice-repellent surface could be realized. Assessed ice shear strength was significantly reduced by more than eight-fold when substrates were coated. The lowest shear strength 105 ± 12 kPa was obtained on the surface with 5 wt% **S17F**. This feature was in the case of the synergism between the migration of **S13F** and **S17F** block copolymer and the PDMS component, endowing the low energy surfaces with high receding water contact angle and very low values of the contact angle hysteresis. Thus, the UV-curable POSS-fluorinated diblock copolymers can be a good candidate for icephobic applications.

Acknowledgments

This work is financially supported by National Natural Science Foundation of China (No. 51273146) and Natural Science Foundation of Tianjin, China (No. 14ZCZDGX00008).

Appendix A. Supplementary data

Supplementary data associated with this article can be found, in the online version, at http://dx.doi.org/10.1016/j.porgcoat.2016.01.005.

References

[1] N. Dalili, A. Edrisy, R. Carriveau, A review of surface engineering issues critical to wind turbine performance, Renew. Sust. Energ. Rev. 13 (2009) 428–438.
[2] X. Wei, Z. Jia, Z. Sun, Z. Guan, M. MacAlpine, Development of anti-icing coatings applied to insulators in China, IEEE Electr. Insul. M. 30 (2014) 42–50.
[3] J. Lv, Y. Song, L. Jiang, J. Wang, Bio-inspired strategies for anti-icing, ACS nano 8 (2014) 3152–3169.
[4] R. Menini, M. Farzaneh, Advanced icephobic coatings, J. Adhes. Sci. Technol. 25 (2012) 971–992.
[5] Q. Fu, X. Wu, D. Kumar, J.W. Ho, P.D. Kanhere, N. Srikanth, E. Liu, P. Wilson, Z. Chen, Development of sol-gel icephobic coatings: effect of surface roughness and surface energy, ACS Appl. Mater. Interfaces 6 (2014) 20685–20692.
[6] M. Susoff, K. Siegmann, C. Pfaffenroth, M. Hirayama, Evaluation of icephobic coatings-screening of different coatings and influence of roughness, Appl. Surf. Sci. 282 (2013) 870–879.
[7] S. Yang, Q.L. Zhu, J. Xue, Q. Wang, Q. Chen, Research on the icephobic properties of fluoropolymer-based materials, Appl. Surf. Sci. 257 (2011) 4956–4962.
[8] H. Sojoudi, G.H. McKinley, K.K. Gleason, Linker-free grafting of fluorinated polymeric cross-linked network bilayers for durable reduction of ice adhesion, Mater. Horiz. 2 (2015) 91–99.
[9] H. Li, X. Li, C. Luo, Y. Zhao, X. Yuan, Icephobicity of polydimethylsiloxane-*b*-poly (fluorinated acrylate), Thin Solid Films 573 (2014) 67–73.
[10] B. Li, X. Li, K. Zhang, H. Li, Y. Zhao, L. Ren, X. Yuan, Synthesis of POSS-containing fluorosilicone block copolymers via RAFT polymerization for application as non-wetting coating materials, Prog. Org. Coat. 78 (2015) 188–199.

[11] K. Honda, M. Morita, H. Otsuka, A. Takahara, Molecular aggregation structure and surface properties of poly (fluoroalkyl acrylate) thin films, Macromolecules 38 (2005) 5699–5705.
[12] K. Honda, M. Morita, O. Sakata, S. Sasaki, A. Takahara, Effect of surface molecular aggregation state and surface molecular motion on wetting behavior of water on poly(fluoroalkyl methacrylate) thin films, Macromolecules 43 (2010) 454–460.
[13] H. Yamaguchi, M. Kikuchi, M. Kobayashi, H. Ogawa, H. Masunaga, O. Sakata, A. Takahara, Influence of molecular weight dispersity of poly{2-(perfluorooctyl)ethyl acrylate} brushes on their molecular aggregation states and wetting behaviour, Macromolecules 45 (2012) 1509–1516.
[14] J. Yang, D. Yuan, B. Zhou, J. Gao, H. Ni, L. Zhang, X. Wang, Studies on the effects of the alkyl group on the surface segregation of poly(n-alkyl methacrylate) end-capped 2-perfluorooctylethyl methacrylate films, J. Colloid Interf. Sci. 359 (2011) 269–278.
[15] W. Zhang, A.H.E. Müller, Architecture, self-assembly and properties of well-defined hybrid polymers based on polyhedral oligomeric silsequioxane (POSS), Prog. Polym. Sci. 38 (2013) 1121–1162.
[16] A.G. Kannan, N.R. Choudhury, N. Dutta, Fluoro-silsesquioxane-urethane hybrid for thin film applications, ACS Appl. Mater. Interfaces 1 (2009) 336–347.
[17] A. Pan, S. Yang, L. He, POSS-tethered fluorinated diblock copolymers with linear- and star-shaped topologies: synthesis, self-assembled films and hydrophobic applications, RSC Adv. 5 (2015) 55048–55058.
[18] X. Li, K. Zhang, Y. Zhao, K. Zhu, X. Yuan, Formation of icephobic film from POSS-containing fluorosilicone multi-block methacrylate copolymers, Prog. Org. Coat. 89 (2015) 150–159.
[19] A.J. Meuler, J.D. Smith, K.K. Varanasi, J.M. Mabry, G.H. McKinley, R.E. Cohen, Relationships between water wettability and ice adhesion, ACS Appl. Mater. Interfaces 2 (2010) 3100–3110.
[20] J. Xiao, S. Chaudhuri, Design of anti-icing coatings using supercooled droplets as nano-to-microscale probes, Langmuir 28 (2012) 4434–4446.
[21] J. Liang, L. He, X. Dong, T. Zhou, Surface self-segregation, wettability, and adsorption behavior of core-shell and pentablock fluorosilicone acrylate copolymers, J. Colloid Interf. Sci. 369 (2012) 435–441.
[22] H. Hussain, S.M. Shah, Recent developments in nanostructured polyhedral oligomeric silsesquioxane-based materials via 'controlled' radical polymerization, Polym. Int. 63 (2014) 835–847.
[23] S.M. Ramirez, Y.J. Diaz, C.M. Sahagun, M.W. Duff, O.B. Lawal, S.T. Iacono, J.M. Mabry, Reversible addition–fragmentation chain transfer (RAFT) copolymerization of fluoroalkyl polyhedral oligomeric silsesquioxane (F-POSS) macromers, Polym. Chem. 4 (2013) 2230–2234.
[24] L. Matějka, M. Janata, J. Pleštil, A. Zhigunov, M. Šlouf, Self-assembly of POSS-containing block copolymers: fixing the hierarchical structure in networks, Polymer 55 (2014) 126–136.
[25] Y. Shao, P. Aizhao, H. Ling, POSS end-capped diblock copolymers: synthesis, micelle self-assembly and properties, J. Colloid Interf. Sci. 425 (2014) 5–11.
[26] D. Yu, Y. Zhao, H. Li, H. Qi, B. Li, X. Yuan, Preparation and evaluation of hydrophobic surfaces of polyacrylate-polydimethylsiloxane copolymers for anti-icing, Prog. Org. Coat. 76 (2013) 1435–1444.
[27] K. Zhang, J. Cai, X. Li, H. Li, Y. Zhao, X. Yuan, Balance of polyacrylate-fluorosilicone block copolymers as icephobic coatings, Chinese J. Polym. Sci. 33 (2014) 153–162.
[28] X. Li, Y. Zhao, H. Li, Y. Xuan, Preparation and icephobic properties of polymethyltrifluoropropylsiloxane-polyacrylate block copolymers, Appl. Surf. Sci. 316 (2014) 222–231.
[29] Y. Gan, X. Jiang, J. Yin, Self-wrinkling patterned surface of photocuring coating induced by the fluorinated POSS containing thiol groups (F-POSS-SH) as the reactive nanoadditive, Macromolecules 45 (2012) 7520–7526.
[30] Y. Gan, J. Yin, X. Jiang, Self-wrinkling induced by the photopolymerization and self-assembly of fluorinated polymer at air/liquid interface, J. Mater. Chem. A. 2 (2014) 18574–18582.
[31] L. Xue, Y. Zhang, Y. Zuo, S. Diao, J. Zhang, S. Feng, Preparation and characterization of novel UV-curing silicone rubber via thiol-ene reaction, Mater. Lett. 106 (2013) 425–427.
[32] K. Goswami, A.L. Skov, A.E. Daugaard, UV-cured, platinum-free, soft poly(dimethylsiloxane) networks, Chem. Eur. J. 20 (2014) 9230–9233.
[33] Y. Mitsukami, M. Donovan, A. Lowe, C. McCormick, Water-soluble polymers. 81. Direct synthesis of hydrophilic styrenic-based homopolymers and block copolymers in aqueous solution via RAFT, Macromolecules 34 (2001) 2248–2256.
[34] W. Shen, Q. Qiu, Y. Wang, M. Miao, B. Li, T. Zhang, A. Cao, Z. An, Hydrazine as a nucleophile and antioxidant for fast aminolysis of RAFT polymers in air, Macromol. Rapid. Comm. 31 (2010) 1444–1448.
[35] M.A. Harvison, T.P. Davis, A.B. Lowe, Macromolecular thiolysis of oxiranes: end-group modification of RAFT prepared homopolymers, Polym. Chem. 2 (2011) 1347–1354.
[36] H. Fang, S. Zhou, L. Wu, Microphase separation behavior on the surfaces of PEG-MDI-PDMS multiblock copolymer coatings, Appl. Surf. Sci. 253 (2006) 2978–2983.
[37] L. Mishchenko, B. Hatton, V. Bahadur, J. Ashley Taylor, T. Krupenkin, J. Aizenberg, Design of ice-free nanostructured surfaces based on repulsion of impacting water droplets, ACS Nano 12 (2010) 7699–7707.
[38] L. Zhu, J. Xue, Y. Wang, Q. Chen, J. Ding, Q. Wang, Ice-phobic coatings based on silicon-oil-infused polydimethylsiloxane, ACS Appl. Mater. Interfaces 5 (2013) 4053–4062.
[39] C. Antonini, F. Villa, I. Bernagozzi, A. Amirfazli, M. Marengo, Drop rebound after impact: the role of the receding contact angle, Langmuir 29 (2013) 16045–16050.
[40] A. Alizadeh, V. Bahadur, S. Zhong, W. Shang, R. Li, J. Ruud, M. Yamada, L. Ge, A. Dhinojwala, M. Sohal, Temperature dependent droplet impact dynamics on flat and textured surfaces, Appl. Phys. Lett. 100 (2012) 111601–111604.
[41] B.B. Wang, Y.P. Zhao, T. Yu, Fabrication of novel superhydrophobic surfaces and droplet bouncing behavior-part 2: water droplet impact experiment on superhydrophobic surfaces constructed using ZnO nanoparticles, J. Adhes. Sci. Technol. 25 (2011) 93–108.
[42] Y.Y. Wang, J. Xue, Q.J. Wang, Q.M. Chen, J.F. Ding, Verification of icephobic/anti-icing properties of a superhydrophobic surface, ACS Appl. Mater. Interfaces 5 (2013) 3370–3381.
[43] C. Wang, T. Fuller, W. Zhang, K.J. Wynne, Thickness dependence of ice removal stress for a polydimethylsiloxane nanocomposite: Sylgard 184, Langmuir 30 (2014) 12819–12826.